Beyond scale separation in gyrokinetic turbulence

X. Garbet [1], Y. Sarazin [1], V. Grandgirard [1], G. Dif-Pradalier [1], G. Darmet [1], Ph. Ghendrih [1], P. Bertrand [2], N. Besse [2], E. Gravier [2], P. Morel [2], E. Sonnendrücker [3], N. Crouseilles [3], J-M. Dischler [4], G. Latu [4], E. Violard [4], M. Brunetti [5], S. Brunner [5], X. Lapillonne [5], T.-M. Tran [5], L. Villard [5]

1) Association Euratom-CEA, CEA/DSM/DRFC Cadarache, France
2) LPMIA -Université Henri Poincaré, Vandœuvre-lès-Nancy, France
3) IRMA -Université de Strasbourg and INRIA Lorraine, France
4) LSIIT -Université de Strasbourg, France
5) CRPP Lausanne, Association EURATOM-Confédération Suisse, Switzerland

E-mail contact: xavier.garbet@cea.fr

Abstract. This paper presents results obtained with a set of gyrokinetic codes with increasing dimensionality and based on a semi-lagrangian scheme. Several physics issues are addressed, namely the comparison between fluid and kinetic descriptions, the intermittent behaviour of flux driven turbulence, the role of zonal flows in transport barriers produced with peaked density profiles, and the role of large scale flows in toroidal ITG turbulence.

1. Introduction

Predicting turbulent transport in nearly collisionless fusion plasmas requires solving the gyrokinetic equations for all species coupled to Maxwell equations. In spite of considerable progress, several pending issues remain. In particular, the choice of the method for solving the Vlasov equation is subject to intense debate. On the one hand, Eulerian codes have proved their efficiency, but are potentially subject to numerical dissipation, therefore requiring high order numerical schemes. On the other hand, Lagrangian codes (typically Particle in Cell codes) benefit from of a widespread experience, but may be affected by numerical noise. The latter problem can be cured by techniques of "optimal loading" and filtering. This paper presents an alternative method based on a semi-Lagrangian scheme [1] applied to gyrokinetics [2,3]. This technique allows to compute the full distribution function with moderate dissipation and has been assessed in several ways. Here, some physics issues are presented, namely the comparison between kinetic and fluid descriptions (including an alternative description based on a Water Bag model), intermittency in flux driven systems, the role of zonal flows in transport barriers produced by large density gradient, and the dynamics of flows in full torus simulations of Ion Temperature Gradient (ITG) turbulence.

2. Reduced 3D simulations: kinetic vs fluid descriptions.

The comparison of fluid and kinetic descriptions has been addressed by studying a 3D kinetic interchange turbulence. This is done by solving the drift-kinetic equation

$$\partial_t F + [\phi, F] + v_d E \partial_y F = 0 \qquad (1)$$

where F is the distribution function, which depends on two spatial dimensions (x,y) (y is 2π periodical) and the energy E. Distances are normalised to a ion thermal gyroradius $\rho_s = m_i v_T / eB_0$ (T_0 and B_0 are reference temperature and magnetic field), $v_T = \sqrt{T_0 / m_i}$ is the thermal velocity), and $[,]$ is a Poisson bracket expressed in x,y coordinates. Self-consistency is ensured by coupling Eq.(1) to the Poisson equation

$$\phi - \langle \phi \rangle - \nabla_\perp^2 \phi = \frac{1}{n_{eq}} \int_0^{+\infty} dE F - 1 \qquad (2)$$

where the bracket indicates an average over the periodic coordinate y. A trapped ion turbulence is also described by Eqs.(1-2) when averaging the Vlasov equation over the fast cyclotron and bounce motions, up to an extra $E^{1/2}$ factor in the expression Eq.(2) of the density [4]. The boundary conditions are such that the distribution function matches a Maxwellian with fixed density and temperature at both ends of the simulation box, while fluctuations are set to zero. The initial distribution function is a Maxwellian with prescribed density and temperatures.

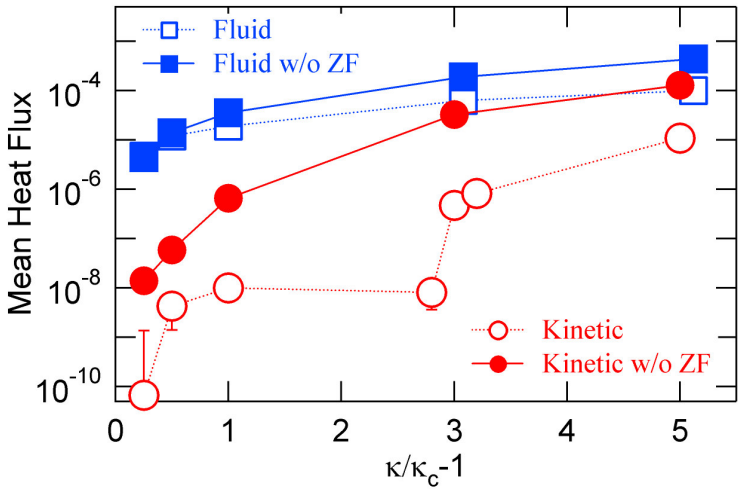

Fig1: Heat flux vs distance to threshold for a 3D kinetic interchange turbulence, with and without zonal flows.

Fluid equations are obtained by computing the two first moments of Eq.(1), i.e.

$$\partial_t N + [\phi, N] + v_d \partial_y P = 0 \quad (3)$$

$$\partial_t P + [\phi, P] + v_d \partial_y Q = 0 \quad (4)$$

where N is the density, P the pressure, and $Q = \int_0^{+\infty} dE E^2 F$ is the heat flux. For kinetic and fluid descriptions to match, an expression for Q, i.e. a closure, must be chosen. The simplest one consists in setting $Q = \Gamma PT$ where Γ is the adiabatic index (for a 2D system, a Maxwellian yields $\Gamma=2$). A well-known drawback of this type of closure is that is does not provide the correct instability threshold. Diffusion can be added to both density and pressure equation to provide a growth rate that is close to the kinetic one. To minimize the numerical errors, the same semi-Lagrangian scheme has been used to solve both the kinetic and fluid equations. For the fluid case, this is done by solving the Vlasov equation for 2 energies $E_\pm$:

$$\partial_t F_\pm + [\phi, F_\pm] + v_d E_\pm \partial_y F_\pm = \nabla \cdot D \nabla F_\pm \quad (5)$$

The density and pressure are defined as $n=F_+ + F_-$ and $P=F_+E_+ + F_-E_-$. In this description, the heat flux is given by $Q=PT+4(E_+ - E_-)^2 F_+F_-/N$. Hence $\Gamma=1$ when E_+ is close to E_-. It is found, as expected, that kinetic fluxes are well below the values calculated in the fluid approach, as shown on Fig.1. This difference is usually explained by the dynamics of zonal flows [5] close to the instability threshold. However this is not the only explanation, as a difference persists when zonal flows are artificially suppressed (see Fig.1). In fact it appears that the distribution function is far from a Maxwellian, and cannot be described by a small number of moments. This observation indicates that wave/particle resonant processes play an important role [6]. It also suggests that most of the closures that have been developed previously will be inefficient in this case. An alternative scheme, based on a Water Bag representation is presented in section 5.

3. Flux driven turbulence.

As mentioned previously, the boundary conditions are such that the system is in contact with two thermal baths at both ends of the simulations box. However a tokamak plasma is flux driven, i.e. the temperature is controlled by a heat source and not by fixed values at the edges. Hence it is quite crucial to study systems where turbulence is flux driven. This has been done for a trapped ion turbulence (equations similar to Eqs.(1-2), [4]) by implementing an energy dependent source term in the Vlasov equation, which is chosen proportional to *E-1*, so that the particle source is null [7]. We single out the evolution of the volume average energies of zonal flow and fluctuating potential (without zonal flows), and a single moment of the distribution function, the temperature. An example of the rich dynamics of these three fields is reported on Fig.2. When a large increase in the magnitude of the zonal flows occurs, the fluctuations are quenched and the core temperature builds-up while the edge temperature decreases (in agreement with the usual picture for a transport barrier). The increase of the temperature gradient through the system takes place at the same time as the magnitude of the zonal flows decays away until an abrupt relaxation event takes place.

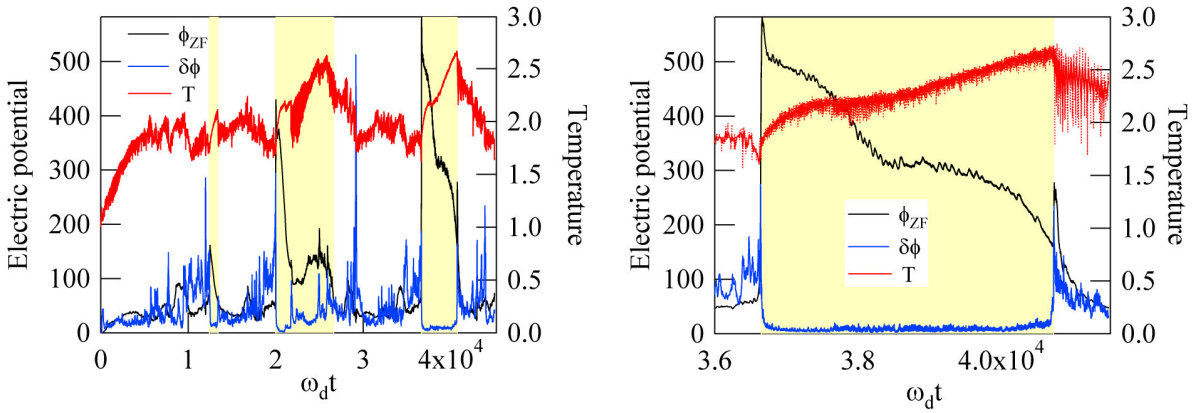

Fig.2:Left panel: time evolution of the volume averaged energy contents of zonal flows, electric potential fluctuations, and central temperature T. Right panel: details of one relaxation (third time window in left panel)

This relaxation governs a significant turbulence mixing during which the zonal flows are reduced, the radial temperature gradient flattens out, and a large energy flux is transferred to the edge (Fig.2, right panel). The zonal flows build-up again, then starting over such a predator-prey cycle. In such simulations the interplay between the zonal flows and the turbulent drift transport generates two distinct behaviours. In some cases there is a strong zonal flow overshoot that generates a transient transport barrier, while in other cases the zonal flows govern a saturation of the turbulent transport. This investigation of flux driven transport in a kinetic simulation confirms previous findings with fluid simulations [8], i.e. that a scale separation assumption is not appropriate with such a realistic drive. It is also consistent with the results obtained in the previous section, i.e. that a reduced description of the velocity space does not capture the right physics of an interchange turbulence described by Eqs.(1-2).

4. Role of zonal flows in transport barriers produced with a peaked density profile.

Slab Ion Temperature Gradient (ITG) driven turbulence has been studied in a cylindrical geometry, using a 4D version of the GYSELA code (3 space coordinates: minor radius *r,* poloidal angle θ , and coordinate along the cylinder axis *z*, plus the velocity along the magnetic field $v_{//}$), which solves the equations:

$$\partial_t F + [\phi, F] + v_{//}\partial_z F - \partial_z \phi \partial_{v_{//}} F = 0 \qquad (6)$$

$$\phi - \langle\phi\rangle - \frac{1}{n_{eq}}\nabla_\perp \cdot \left(n_{eq}\nabla_\perp \phi\right) = \frac{1}{n_{eq}}\int dv_{//} F - 1 \qquad (7)$$

It turns out that the non linear evolution of this system depends strongly on the initial density profile n_{eq} [9]. When the initial density profile is flat, the temperature profile evolves towards a state where its gradient is weak, i.e. with low confinement (see Fig.3). On the other hand, for a peaked initial density profile, the temperature profile steepens, i.e. a transport barrier develops (Fig.3). It is well known that a large density gradient is linearly stabilizing for slab ITG modes (the stability diagram is shown on Fig.4). However this is not the main ingredient. Indeed zonal flows appear to play a crucial role in the development of the transport barrier.

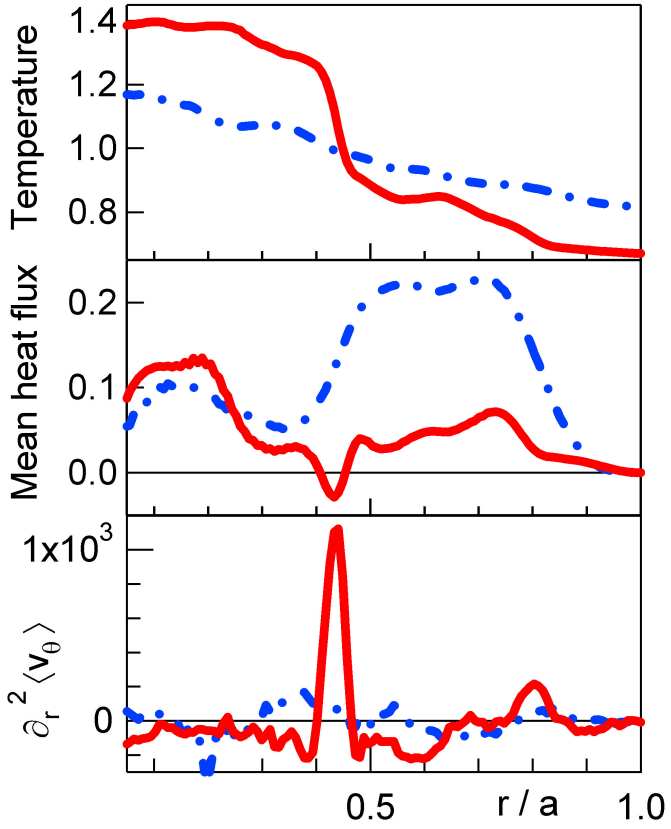

Fig.3: Final profiles of temperature, turbulent flux, and zonal flow shearing rate for flat (dot-dashed) and peaked (plain line) density profiles

The difference of behaviour between peaked and flat density profiles can be understood by analysing the mechanism of turbulent flow generation in presence of a density gradient. The evolution of the mean poloidal velocity is given by the equation

$$\partial_t \langle v_\theta \rangle = -r^{-2}\partial_r \left(r^2 \Pi\right) - \frac{\partial_r n_{eq}}{n_{eq}}\Pi \qquad (8)$$

where $\Pi = \langle v_{E\theta} v_{Er} \rangle$ is the Reynolds stress tensor. The second term in the r.h.s. of Eq.(8) is usually small when compared to the first term. Nevertheless the divergence of the Reynolds stress is found to depend sensitively on the density gradient. A quasi-linear calculation yields the following expression

$$\Pi = \frac{\sqrt{3}}{4}\frac{L_T}{L_w^2}\left(1 - \frac{L_T}{2L_w}\right)\sum_{k_\theta k_z \omega}\frac{v_T}{|\omega|}\left|\frac{k_\theta \phi_{k\omega}}{B}\right|^2 \qquad (9)$$

where $w = n_{eq} - \partial_r \left(r n_{eq} \langle v_\theta \rangle \right)$ is the density of gyrocenters (in practice a potential vorticity), L_w is the corresponding gradient length. Hence a strong density gradient leads to large values of the stress tensor. This result is consistent with the numerical findings. Quite interestingly, it is found that the barrier is located in an extremum of flow curvature, rather than flow shear. This property is recovered by analysing the stability in presence of a slowly varying shear flow. A Schrödinger-like equation can be written for a mode radial structure, whose effective potential depends on the flow curvature. If a maximum of flow curvature is located at a maximum of temperature gradient, the potential exhibits an anti-well structure that expels the modes from this region, and therefore likely leads to a low level of turbulent transport [9].

5. An alternative approach to kinetic vs fluid descriptions: the Water Bag model

The Water Bag model provides the bridge between kinetic and fluid descriptions. It gives an interesting alternative to the usual kinetic description, using the conservation property of the distribution function in the phase space. Accordingly, a discrete distribution function is assumed along the velocity direction, taking the form of a multi-step-like function. Water Bag model were previously used only for non magnetised plasmas because this model is well suited only for problems involving phase space with one velocity component. This model is applied for the first time to ITG modes in a cylinder, described by Eqs.(6-7). A linear analysis has been achieved, which provide the local dispersion relation of a drift-kinetic Multi Water Bag plasma :

$$\varepsilon(\omega) = 0 = 1 + \frac{Z_i}{\tau} \sum_{j=1}^{N} \frac{\omega(\beta_j \Omega_T^* + \gamma_j \Omega_n^*) - \alpha_j}{\omega^2 - a_j^2} \qquad (10)$$

where $\alpha_j, \beta_j, \gamma_j$ are related to density of the jth bag, a_j is its equilibrium parallel velocity, N is the number of bag, Z_i the ionic charge number, $\tau = T_i/T_e$ the ratio of ion to electron temperatures, Ω_T^* and Ω_n^* the diamagnetic frequencies related to the temperature and density gradients.

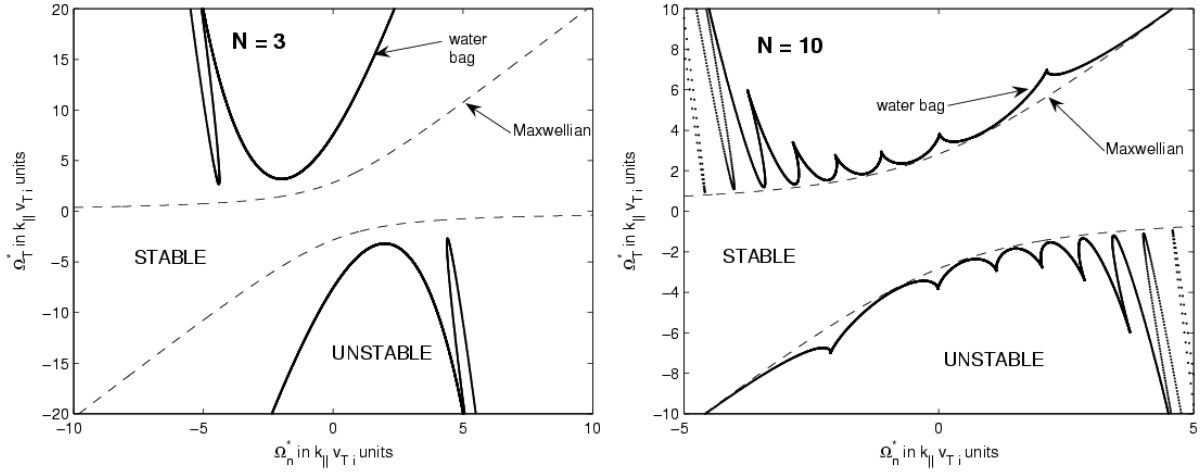

Fig.4: Instability diagram in the plane $\Omega_T^* = f(\Omega_n^*)$. Comparison between a Multi Water Bag distribution function and a Maxwellian.

Finding the complex roots of Eq.(10) provides the linear growth rate, whose existence and value essentially depend on the values of the temperature and density gradients (respectively Ω_T^* and Ω_n^*). The one bag case is shown to be equivalent to the adiabatic fluid description, without any instability, and a constant ratio between temperature and density gradients ($L_n/L_T=2$). The instability threshold for ITG instability is found to be very close to the results

obtained from continuous Maxwellian distribution function (see Fig.4), even for a number of bags as small as 10 [10].

6. Global non perturbative simulations of toroidal ITG turbulence

The GYSELA code has been upgraded to run 5D simulations of toroidal ITG turbulence [11]. The codes solves the gyrokinetic equation

$$\partial_t F + \boldsymbol{v_E} \cdot \nabla F + \boldsymbol{v}_g \cdot \nabla F + v_{//} \nabla_{//} F - \dot{v}_{//} \partial_{v_{//}} F = 0 \tag{11}$$

where

$$\boldsymbol{v}_E = \frac{\boldsymbol{B} \times \nabla (J \cdot \phi)}{B^2} \quad ; \quad \boldsymbol{v}_g = \frac{m v_{//}^2}{eB} \left(\frac{\boldsymbol{B}}{B} \times \frac{\boldsymbol{N}}{\mathrm{R}} \right) + \frac{\mu}{e} \left(\frac{\boldsymbol{B}}{B} \times \frac{\nabla B}{B} \right) \tag{12}$$

$$m \dot{v}_{//} = - \left[\frac{\boldsymbol{B}}{B} + \frac{m v_{//}}{eB} \left(\frac{\boldsymbol{B}}{B} \times \frac{\boldsymbol{N}}{\mathrm{R}} \right) \right] . \left(\mu \nabla B + e \nabla J . \phi \right) \tag{13}$$

The Poisson equation reads

$$\phi - \langle \phi \rangle - \frac{1}{n_{eq}} \nabla_\perp \cdot \left(n_{eq} \nabla_\perp \phi \right) = \frac{1}{n_{eq}} \int B d\mu dv_{//} J \cdot F - 1 \tag{14}$$

where J is the gyroaverage operator (multiplication by $J_0(k_\perp \rho_c)$ in Fourier space, ρ_c is the gyroradius). The code uses a simplified geometry based on a set of circular centered magnetic surfaces with a magnetic field $\boldsymbol{B}=B_0R_0/R(\boldsymbol{e}_\varphi+r/qR_0\boldsymbol{e}_\theta)$ and $R=R_0+rcos(\theta)$. The parameters of the simulation corresponds to the Cyclone base case [5] with a gyroradius normalised to the bow size ρ_* equal to 0.01. Several numerical tests have been done to check the accuracy when solving the Vlasov equation, in particular the conservation of motion invariants [11]. It is also found that the linear growth rate agrees well with the expected values. Moreover it has been verified that the electric potential ϕ_{00} evolves as prescribed by Rosenbluth and Hinton [12], i.e. decays and saturates at a non zero residual value.

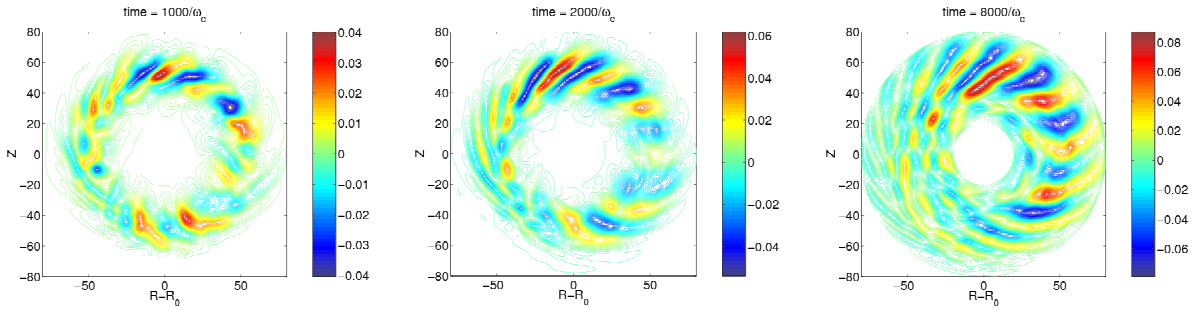

Fig.5: Contour lines of the electric potential in a poloidal cross section for an ITG turbulence simulation when zonal flows are artificially suppressed.

In the case where the $n=0,m=0$ component ϕ_{00} of the electric potential is artificially suppressed and the initial distribution function is a Maxwellian of the form

$$F_{eq}(r,E) = \frac{n_{eq}(r)}{\left[2\pi m T_{eq}(r) \right]^{3/2}} exp\left\{ - \frac{E}{T_{eq}(r)} \right\} \tag{15}$$

where $E = m v_{//}^2 / 2 + \mu B$, a standard ITG turbulence develops, as shown in Fig.5. However if ϕ_{00} is self-consistently calculated, large scale steady flows appear, which prevent the onset of turbulence. This is a consequence of the equilibrium distribution function not being a function

of the motion invariants. If the distribution function is a function of the minor radius instead of the canonical toroidal moment, no parallel flow exists initially to balance the charge separation associated to ion curvature drift. Hence a polarisation drift appears to ensure the charge balance. Parallel flows develop in a second stage, but the shear flow is too strong to allow a growth of turbulence. This problem was already mentioned by Idomura et al. [13] and by Angelino et al. [14]. It is cured by using the prescription proposed in the latter reference, i.e. prescribing an equilibrium distribution function of the form Eq.(15), with the radius r replaced by the motion invariant $\bar{r}$ defined as [14]

$$\bar{r} = r_0 - \frac{q_0}{r_0}\int_{r_0}^{r}\frac{r dr}{q} + \frac{q_0}{r_0}\frac{m}{eB_0}\left(Rv_{//} - R_0\bar{v}_{//}\right) \tag{16}$$

where

$$\bar{v}_{//} = sign(v_{//})\left[\frac{2}{m}\left(E-\mu B_{\max}\right)\right]^{1/2} Y\left(E-\mu B_{\max}\right) \tag{17}$$

and Y is a step function, B_{max} is the maximum of magnetic field in the whole box (all quantities with a label 0 are defined at half-radius of the simulation box). With this prescription, the average parallel velocity and electric potential evolve towards steady values. The final state is turbulent, and the level of fluctuations $e(\phi-\phi_{eq})/T_{eq}$ lies in the expected range (Fig. 6).

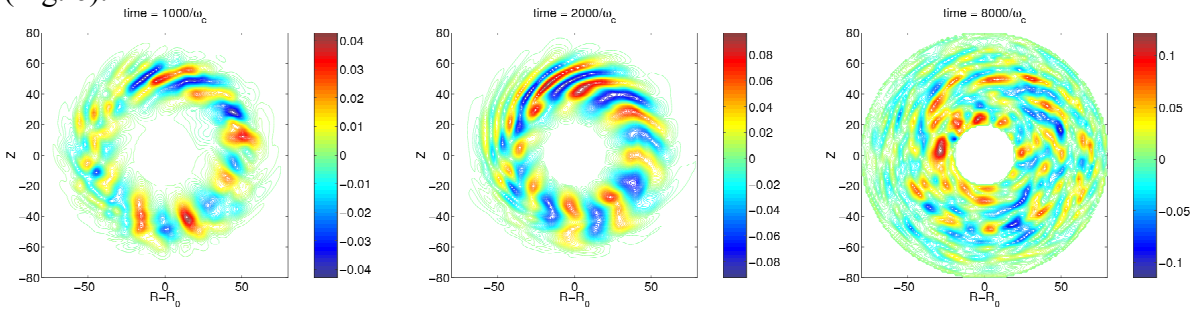

Fig.6: Contour lines of the fluctuations of electric potential $e(\phi-\phi_{eq})/T_{eq}$ for ITG turbulence with zonal flows when the initial distribution function is canonical.

In fact, the prescription (16-17) belongs to a larger class of distribution functions [15], defined for a general magnetic field $\boldsymbol{B}=I(\psi)\,\boldsymbol{\nabla}\varphi+\boldsymbol{\nabla}\psi\times\boldsymbol{\nabla}\varphi$ as

$$F_{eq}(\bar{\psi},E,w_{//}) = \frac{n_{eq}\,exp\left(e\phi_{eq}/T_{eq}\right)}{\left[2\pi m T_{eq}\right]^{3/2}} exp\left\{-\frac{E}{T_{eq}}\right\}\left\{1+\frac{m w_{//} W_{// eq}}{T_{eq}}\right\} \tag{18}$$

where n_{eq}, T_{eq}, and $W_{//eq}$, are functions of the motion invariant $\bar{\psi} = \psi + mIv_{//}/eB$, $E = mv_{//}^2/2 + \mu B + e\phi_{eq}$ is the energy and $w_{//}$ is a motion invariant related to the parallel velocity, i.e.

$$w_{//} = sign(v_{//})\left[\frac{2}{m}\left(E-\mu B_{\max}\right)\right]^{1/2} Y\left(E-\mu B_{\max}\right) \quad ; \quad B_{\max} = B(\bar{\psi},\theta=\pi) \tag{19}$$

Developing Eq.(18) at first order in ρ_* and calculating the 2nd moment yield the fluid velocity

$$\boldsymbol{V} = W_{// eq}(\psi)\frac{\boldsymbol{B}}{B_{max}(\psi)} + \left(\frac{d\phi_{eq}}{d\psi} + \frac{1}{n_{eq}e}\frac{dp_{eq}}{d\psi}\right)R^2\nabla\varphi \tag{20}$$

This expression is fully consistent with the usual prescription for the equilibrium velocity in a tokamak, and satisfies the force balance equation $\boldsymbol{E}+\boldsymbol{V}\times\boldsymbol{B}-\boldsymbol{\nabla}p/ne=0$. In a collisionless code, the choice of the function $W_{//eq}$ is arbitrary. The choice (16-17) minimizes the mean parallel

velocity, as mentioned in ref. [14]. Adding collisions would lead to a different result as the neoclassical viscous damping prescribes a value of $W_{//eq}$ that usually corresponds to a finite parallel velocity. Hence the choice of the initial distribution function is intimately related to the structure of the initial mean flow.

7. Conclusion

A sequence of gyrokinetic codes with increasing dimensionality and based on semi-lagrangian scheme has been developed and used to clarify several physics issues related to the interplay between flows and turbulence, and the scale separation assumption. Turbulent fluxes for a 3D interchange turbulence are found to be different when using fluid or kinetic equations. This discrepancy is partially due to the different behaviour of zonal flows. In fact the distribution function is found to be far from a Maxwellian, suggesting that part of the difference is due to resonant wave/particle interaction. Flux driven interchange turbulence has also been simulated. As in previous fluid flux-driven simulations, strong intermittency is observed. It is related to abrupt relaxations of the temperature profile, correlated with fast events in the zonal flow and fluctuation dynamics. ITG turbulence in a cylinder has been studied with the 4D GYSELA code. A strong density gradient leads to the formation of a transport barrier. Linear stability is not the main reason for this behaviour, which is rather due to the dynamics of zonal flows. For the same 4D system, an alternative to fluid and kinetic description, the Water Bag representation, has been studied. It is shown to reproduce correctly the kinetic linear growth rate and frequencies with a limited amount of bags. Finally a 5D version of the GYSELA code has been developed to study a toroidal ITG turbulence. The linear growth rates agree with the values expected for the Cyclone base case and zonal flows behave as expected. The choice of the initial distribution function is crucial for the non linear stage. It has to be a function of motion invariants as any other choice leads to the development of large scale flows, which prevent the onset of turbulence.

References

[1] E. Sonnendrücker, J. Roche, P. Bertrand, A. Ghizzo J. Comp. Physics **149**, 201 (1999).
[2] M. Brunetti, V. Grandgirard, O. Sauter, J. Vaclavik, L. Villard, Comput. Phys. Commun. **163**, 1 (2004).
[3] V. Grandgirard et al., J. Comp. Physics **217**, 395 (2006).
[4] G. Depret et al., Plasma Phys. and Control. Fusion **42**, 949 (2000).
[5] A.M. Dimits et al. , Phys. Plasmas 7, 969 (2000).
[6] Y. Sarazin et al. Plasma Phys. Control. Fusion **47**, 1817 (2005).
[7] G. Darmet et al., in Proceedings of the Vlasovia conference, 2006.
[8]Ph. Ghendrih et al., Journal of Nuclear Materials **337–339,** 347 (2005).
[9] Y. Sarazin et al., Phys. Plasmas **13**, 092307 (2006).
[10] P. Morel, E. Gravier, N. Besse, P. Bertrand, "The Water Bag model for gyrokinetic simulations", in Proc. of 33rd EPS Conference on Plasma Physics (2006)
[11] V. Grandgirard et al., in Proc. of International Theory Conference, Varenna (2006).
[12] M. N. Rosenbluth and F.L. Hinton Phys. Rev. Lett. **80**, 724 (1998).
[13] Y. Idomura et al., Nucl. Fusion **43**, 234 (2003).
[14] P. Angelino et al., Phys. Plasmas **13**, 052304 (2006).
[15] G. Dif-Pradalier et al., in Proceedings of the Vlasovia conference, 2006.